Analytical steady-state model based on Fourier integral transforms for cylindrical heat pipes under axisymetric conditions

Nicolas Blet, Denis Maillet

Version of Record: https://www.sciencedirect.com/science/article/pii/S0017931021012230
Manuscript_cbb3e653feca9733a773dd414c041dcf

Analytical steady-state model based on Fourier integral transforms for cylindrical heat pipes under axisymetric conditions

Nicolas Blet*, Denis Maillet

Université de Lorraine, CNRS, LEMTA, F-54000 Nancy, France

Abstract

A thermohydraulic analytical model of a capillary cylindrical heat pipe in steady-state is proposed in this article. It is based on an original representation by thermal quadrupoles to describe heat transfer in the wall and in the porous wick, via the use of Fourier integral transforms. Thanks to a validation from literature results, this model provides two-dimensional axisymetric thermal fields and one-dimensional pressure and velocity profiles of both liquid and vapour flows. Different developments and solutions are introduced according to the kind of boundary conditions at evaporator and at condenser, and with a more or less strong thermohydraulic coupling at the liquid/vapour interface. For the simple case with imposed uniform heat fluxes, intrinsic properties of the heat pipe are originally defined. The introduced model offers a generalisation of analytical models of standard heat pipe as a design or optimisation tool. Wider developments of analytical models for more complex three-dimensional geometries of heat pipe and in transient regime can be expected.

Keywords: Cylindrical heat pipe, Steady-state analytical model, Thermal quadrupoles, Thermohydraulic coupling

1. Introduction

Many modelling developments and analyses of heat pipes have been carried out and can be found nowadays, thanks to the increase of application opportunities, either to improve heat transfer (electronic cooling, ...) or to reduce thermal gradients [1]. While some modelling improvements still remain for loop heat pipes and pulsating heat pipes, much work has already been done to develop sizing or analysis tools for capillary heat pipes.

Today, numerical studies are often selected to study precise thermohydraulic effects in the vapour flow or in the liquid flow in the porous media, but some analytical developments can be found, even in recent years. While sizing models were firstly focused on hydraulic considerations, that is evaluating a capillary limit from liquid and vapour pressure drops [2], more precise thermal models have been introduced now.

Zuo and Faghri [3] propose a transient thermal network to describe the behaviour of a standard cylindrical heat pipe through simple radial or axial thermal resistances. Solving the ordinary differential equations system is done by numerical standard Runge-Kutta method. From boundary conditions, the operating temperature of the heat pipe can be evaluated in particular. With Darcian pressure drops for the vapour and liquid flows and from the Clausius-Clapeyron equation, a dimensionless criterion of "thermal compatibility" is proposed between the geometric parameters of the heat pipe, the thermal conductivity of the material and the fluid properties.

Zhu and Vafai [4] focus on an analytic development of velocity and pressure profiles of the vapour and liquid flows in a cylindrical heat pipe under axisymetric boundary conditions in steady-state. In particular, non-Darcian transport and interfacial effects are taken into account. The method of matched asymptotic expansions is used to obtain a closed-form solution. Assuming that the vapour phase is saturated with a uniform temperature along

*Corresponding author
Email address: nicolas.blet@univ-lorraine.fr (Nicolas Blet)

the heat pipe, the external wall temperature profile is obtained by a simple radial heat conduction model without heat losses, from the heat input at evaporator and the coolant temperature at condenser.

In the case where the capillary structure is merely grooves in the heat pipe wall, some specific modelling have been also developed. For example, Kim and Seo [5] propose a mathematical model to evaluate the maximum heat transport capability of a miniature heat pipe with a special shape grooved wick structure. From continuity and momentum balances of the vapour and liquid flows, the evaluation of the axial evolution of the interface curvature and the liquid block length at condenser are assessed first. A mean thermal resistance of the heat pipe is then calculated from mean resistances specific to heat transfer at evaporator, to the evolution of the saturated vapour temperature and to heat transfer at condenser, according to the various liquid levels in the grooves at both evaporator and condenser.

In 2011, Aghvami and Faghri [6] introduce a two-dimensional analytical thermohydraulic model for flat heat pipes with various sollicitation configurations in steady state. Temperature field in the wall of the heat pipe are evaluated under the form of infinite Fourier cosine series, with coefficients under exponential form. A constant saturation temperature is imposed at the liquid/vapour interface and a linear temperature profile across the wick structure is assumed, through an equivalent thermal conductivity. The velocity and pressure distributions for the vapour flow and for the liquid flow are obtained thanks to the assumption of a parabolic velocity profile. The overheating of the vapour is then evaluated from the Clapeyron equation and the effective capillary pressure is deduced. In a parallel work, Shabgard and Faghri [7] propose an equivalent analytical model for capillary cylindrical heat pipes. With the same assumptions, two-dimensional wall temperature field, and velocity and pressure profiles for vapour and liquid flows are written under the form of infinite series of products of cosine and modified Bessel functions. All the analytical results are compared with full numerical simulations. From a parametric analysis, Shabgard and Faghri propose an improvement of the previous equivalent thermal networks by introducing some additional thermal resistances for a better consideration of axial heat transfer in the wall, which is not necessarily negligible in certain cases, especially in the calculation of the pressure drops in the heat pipe. In 2014, Lips and Lefèvre [8] generalise this kind of approach by introducing an analytical design model for flat and cylindrical capillary heat pipes. Three-dimensional calculations are here made with double Fourier cosine and sine series. The thermal problem of the cylindrical case is solved in rectangular coordinates as well as in the flat case, by assuming a thin thickness for the wall with respect to the perimeter of the heat pipe. An imposed uniform saturation temperature and imposed heat fluxes at evaporator and at condenser are taken as boundary conditions.

In the last years, full numerical analyses have been achieved. Three-dimensional thermohydraulic solving is performed by the finite volume method [9, 10], by finite elements [11] or by the more recent Lattice-Boltzmann method [12]. The main disadvantage of these numerical modelling is naturally the long duration of the calculation compared to previous analytical models. Simulation time of several hours are needed against few seconds for the calculation of analytical Fourier series (with 200 terms) [7]. So, even if some additional assumptions are required with some small inaccuracies, the analytical models are always interesting in order to develop a fast and quite accurate design tool for a capillary heat pipe. The present article introduces thus a generalisation of the analytical approach by Fourier series [6, 7, 8] for a capillary cylindric heat pipe via an original mathematical representation by thermal quadrupoles.

2. Problem description

The developed model is focused in this article on the standard axisymetric problem of a capillary cylindrical heat pipe in steady state. The heat source and the heat sink can be either located at each extremity (Fig. 1) for usual applications or anywhere along the axis. The problem of multi-sources positioning of the x axis can even be considered. The only constraint is to consider these sources as uniform around the axis of the heat pipe. Furthermore, the studied heat pipe is composed of a hollow tube with an inner porous layer, but the model can be extended to a heat pipe with several porous layers.

The considered problem relies on the following assumptions, mainly posed for an achievable analytical solution:

- the vapour and liquid flows are considered unidirectional along the x axis ;
- the vapour flow is supposed at saturation with a parabolic axial velocity profile ;

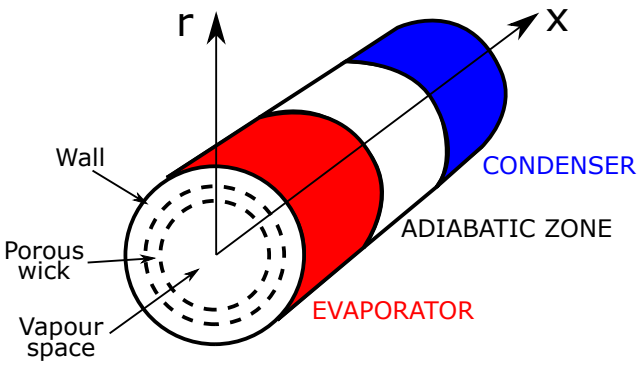

Figure 1: Heat pipe geometry

- 2D-axisymetric heat transfer by conduction in the wall of the pipe and in the porous wick are taken into account ;
- the thermodynamic properties of the fluid and of the solid parts are supposed constant ; properties of the vapour and of the liquid are assumed to be evaluated at the mean saturation temperature at the liquid/vapour interface along the heat pipe ; due to a low velocity liquid flow, an equivalent thermal conductivity λ_{eq} is assumed for the capillary structure full of liquid. In the literrature, different formulations can be found to determine it, according to the fluid-material pair and the kind of capillary structure [13]. For example, for a wrapped screen [14], λ_{eq} can be evaluated by:

$$\lambda_{eq} = \frac{\lambda_l\left[\lambda_l + \lambda_w - (1-\epsilon_w)(\lambda_l - \lambda_w)\right]}{\lambda_l + \lambda_w + (1-\epsilon_w)(\lambda_l + \lambda_w)} \tag{1}$$

  where ϵ_w is the porosity of the wick ;
- the heat pipe operation is supposed to be regular : the liquid/vapour interface is located at the inner diameter, corresponding to the vapour domain, and no thermal effect of the interface curvature or of a possible liquid slug is considered.

In the rest of the document, the solid geometry of the heat pipe will be defined by the axial abscissa x from 0 to the length of the heat pipe L, and by the radius abscissa r varying from the inner radius R_i of the vapour domain to the outer radius R_o of the solid wall. The radial location of the contact between the wall and the porous wick is noted R_w.

The following boundary conditions for the global problem are considered (they correspond to the most standard conditions met in the literature):

- the heat pipe is insulated at each extremity, $x = 0$ and $x = L$;
- a heat flux q_E is imposed at the evaporator ; according to axisymetric assumptions, q_E can only depend on x ;
- a condition of convection is considered at the condenser, with a reference temperature T_C and a heat transfer coefficient h_C ;
- heat losses with ambience can be taken into account at a temperature T_∞ through a heat transfer coefficient h_∞.

Some of these conditions could be simplified according to cases considered in the next sections.

With these external conditions, different models are developed depending on the coupling between thermal model and hydraulic model (with or without the assumption of a uniform saturation temperature for the evaluation of heat transfer) and on the considered vapour pressure drop (with or without non-linear dynamic pressure drop).

3. Model development

3.1. Thermal model

Heat equations in the two layers (solid and porous wick) are simply defined in steady state by the Laplace equation, written in cylindrical coordinates:

$$\frac{\partial^2 T}{\partial x^2} + \frac{1}{r}\frac{\partial}{\partial r}\left(r\frac{\partial T}{\partial r}\right) = 0 \tag{2}$$

To solve more easily this Laplace equation, it is interesting to work with temperature variation around a reference temperature, rather than directly with absolute temperature. In our case, a good idea is to take the reference temperature as the mean fluid saturation temperature in the axis direction and at $r = R_i$, noted $\overline{T}_{sat}$. So we pose thereafter $\theta = T - \overline{T}_{sat}$. The heat equation is then written:

$$\nabla^2\theta = 0 \tag{3}$$

The adiabatic boundary conditions at $x = 0$ and $x = L$ are written:

$$\left.\frac{\partial\theta}{\partial x}\right|_{x=0} = \left.\frac{\partial\theta}{\partial x}\right|_{x=L} = 0 \tag{4}$$

Due to these conditions, the Fourier integral transform of θ, noted $\tilde{\theta}_n$, relative to the space variable $x \in [0; L]$, is defined as:

$$\tilde{\theta}_n(r) = \int_0^L \theta(x,r)cos(\alpha_n x)dx \tag{5}$$

where the eigenvalues α_n are defined for any natural number n by $\alpha_n = n\pi/L$. The associated inverse transform for returning to the original domain is:

$$\theta(x,r) = \frac{\tilde{\theta}_0(r)}{L} + \frac{2}{L}\sum_{n=1}^{\infty}\tilde{\theta}_n(r)cos(\alpha_n x) \tag{6}$$

The integral tranforms of the heat equation (3), taking into account boundary conditions (4), become:

- for the fundamental eigenvalue ($n = 0$):

$$\frac{1}{r}\frac{d}{dr}\left(r\frac{d\tilde{\theta}_0}{dr}\right) = 0 \tag{7}$$

- for the harmonic eigenvalues ($n > 0$):

$$\frac{1}{r}\frac{d}{dr}\left(r\frac{d\tilde{\theta}_n}{dr}\right) - \alpha_n^2\tilde{\theta}_n = 0 \tag{8}$$

Introduction of the integral transform of the rate of heat flux through a cylindrical surface, per unit length in the axial direction, $\phi = -2\pi r\lambda\partial\theta/\partial r$, makes a corresponding quadrupole form possible for a layer with constant thermal conductivity located between two radii R_1 and R_2:

$$\begin{pmatrix}\tilde{\theta}_n\\ \tilde{\phi}_n\end{pmatrix}_{r=R_2} = \begin{pmatrix}A_n & B_n\\ C_n & D_n\end{pmatrix}\begin{pmatrix}\tilde{\theta}_n\\ \tilde{\phi}_n\end{pmatrix}_{r=R_1} \tag{9}$$

Notation	Expression
A_0	1
B_0	$ln\left(R_1/R_2\right)/(2\pi\lambda)$
C_0	0
D_0	1
A_n	$\alpha_n R_1[I_0(\alpha_n R_2)K_1(\alpha_n R_1)+I_1(\alpha_n R_1)K_0(\alpha_n R_2)]$
B_n	$[I_0(\alpha_n R_1)K_0(\alpha_n R_2)-I_0(\alpha_n R_2)K_0(\alpha_n R_1)]/(2\pi\lambda)$
C_n	$2\pi\lambda\alpha_n^2 R_1 R_2[I_1(\alpha_n R_1)K_1(\alpha_n R_2)-I_1(\alpha_n R_2)K_1(\alpha_n R_1)]$
D_n	$\alpha_n R_2[I_0(\alpha_n R_1)K_1(\alpha_n R_2)+I_1(\alpha_n R_2)K_0(\alpha_n R_1)]$
I_0, I_1 and K_0, K_1 are the modified Bessel functions of zero and first order, respectively, of first and second kind	

Table 1: Quadrupole coefficients in cylindrical coordinates

where the matrix coefficients A_n, B_n, C_n and D_n are defined in Table 1 [15]. It has to be noted that the coefficient B_0 corresponds to the radial conductive resistance, and so the two fundamental scalar equations above correspond to a one-dimensional model.

The two-layers conductive problem can also be written under the quadrupole form, linking both interfaces $r = R_i$ and $r = R_o$:

$$\begin{pmatrix}\tilde{\theta}_n\\ \tilde{\phi}_n\end{pmatrix}_{r=R_o}=\begin{pmatrix}\mathbb{A}_n & \mathbb{B}_n\\ \mathbb{C}_n & \mathbb{D}_n\end{pmatrix}\begin{pmatrix}\tilde{\theta}_n\\ \tilde{\phi}_n\end{pmatrix}_{r=R_i} \tag{10}$$

where the quadrupole matrix is the product of the two matrices related to each of the two layers.

3.2. Thermodynamic considerations at the liquid/vapour interface

The boundary condition at $r = R_i$ corresponds to the liquid/vapour interface.

3.2.1. Thermal conditions

By definition of the mean vapour temperature $\overline{T}_{sat}$, the fundamental $\tilde{\theta}_0\big|_{r=R_i}$ is null.

Furthermore, a heat balance written for the whole vapour domain implies :

$$\int_0^L \phi\big|_{r=R_i}=0 \Rightarrow \tilde{\phi}_0\big|_{r=R_i}=0 \tag{11}$$

3.2.2. Thermodynamic condition of saturation

As a first approximation, the saturation temperature variation along the heat pipe can be neglected for the estimation of the heat transfer, typically when the vapour pressure drop is small compared to the variation of the saturation pressure, for example with a large vapour diameter. In that case, it implies in addition :

$$\tilde{\theta}_n\big|_{r=R_i}=0 \tag{12}$$

However, in order to have a stronger coupling between heat transfer and hydraulics, for example for heat pipes with smaller vapour space, it can be interesting to take into account the axial variation of the saturation temperature.

The idea of the model is to linearise the saturation equation near the mean temperature $\overline{T}_{sat}$:

$$\frac{dP_v}{dT_v}=K_{sat} \tag{13}$$

where K_{sat} is a constant depending on $\overline{T}_{sat}$ only.

This linearisation implies the relationship :

$$P_v-P_{sat}(\overline{T}_{sat})=K_{sat}\,\theta|_{r=R_i} \tag{14}$$

and so the mean vapour pressure is equal to the saturation pressure at $\overline{T}_{sat}$.

3.3. Hydrodynamic model

3.3.1. Vapour flow

Velocity profile.

The axial velocity profile of the vapour flow is assumed to be parabolic. With symetry at $r = 0$ and slip condition at the interface ($r = R_i$) [7], it is expressed as:

$$u_x(x,r) = 2u_v(x)\left(1 - \frac{r^2}{R_i^2}\right) \tag{15}$$

where $u_v(x)$ is the mean vapour velocity defined by:

$$u_v(x) = \frac{2}{R_i^2}\int_0^{R_i} r\,u_x(x,r)\,dr \tag{16}$$

The mass balance is written:

$$r\frac{\partial u_x}{\partial x} + \frac{\partial (r\,u_r)}{\partial r} = 0 \tag{17}$$

Integrating Eq. (17) between 0 and r provides the expression of the radial velocity:

$$u_r(x,r) = -\frac{du_v}{dx}\,r\left(1 - \frac{r^2}{2R_i^2}\right) \tag{18}$$

At $r = R_i$, assuming that conductive effects are negligible compared to phase change, the balance at the interface gives the relation between the mean velocity and heat flux:

$$\frac{du_v}{dx} = \frac{-\phi\big|_{r=R_i}}{\pi\rho_v h_{lv} R_i^2} \tag{19}$$

Integrating Eq. (19) between 0 and x, and developing the Fourier series of $\phi\big|_{r=R_i}$, the mean velocity of vapour is finally expressed as:

$$u_v(x) = \frac{-2}{\pi\rho_v h_{lv} R_i^2 L}\sum_{n=1}^{\infty}\frac{\tilde{\phi}_n\big|_{r=R_i}}{\alpha_n}\,sin(\alpha_n x) \tag{20}$$

Pressure profile.

The momentum balance of the vapour flow is written assuming that pressure variations are unidirectional following x:

$$\frac{\partial P_v}{\partial x} = \mu_v\left(\frac{1}{r}\frac{\partial}{\partial r}\left(r\frac{\partial u_x}{\partial r}\right) + \frac{\partial^2 u_x}{\partial x^2}\right) - \rho_v\left(u_r\frac{\partial u_x}{\partial r} + u_x\frac{\partial u_x}{\partial x}\right) \tag{21}$$

Thanks to expressions of axial and radial velocities (Eqs (15) and (18)), integrating Eq. (21) between 0 and R_i gives:

$$\frac{dP_v}{dx} = \frac{-8\mu_v}{R_i^2}u_v + \mu_v\frac{d^2u_v}{dx^2} - \frac{4}{3}\rho_v\frac{du_v^2}{dx} \tag{22}$$

Integrating Eq. (22) between 0 and x and introducing the mean vapour pressure result in a vapour pressure profile that can be expressed by:

$$P_v(x) = P_{sat}(\overline{T}_{sat}) + \frac{8\mu_v}{R_i^2}\left(\frac{1}{L}\int_0^L\int_0^x u_v(x')dx'dx - \int_0^x u_v(x')dx'\right) + \mu_v\frac{du_v}{dx} + \frac{4}{3}\rho_v\left(\frac{1}{L}\int_0^L u_v^2(x)dx - u_v^2(x)\right) \tag{23}$$

From the expression of the mean vapour velocity (20), Eq. (23) finally gives:

$$P_v(x) = P_{sat}(\overline{T}_{sat}) - \frac{16\mu_v}{\pi\rho_v h_{lv} R_i^4 L}\sum_{n=1}^{\infty}\left(\frac{1}{\alpha_n^2} + \frac{R_i^2}{8}\right)\tilde{\phi}_n\big|_{r=R_i}\,cos(\alpha_n x) + \frac{16}{3\pi^2\rho_v h_{lv}^2 R_i^4 L^2}\left(\frac{1}{2}\sum_{n=1}^{\infty}\frac{\tilde{\phi}_n^2\big|_{r=R_i}}{\alpha_n^2} - \left(\sum_{n=1}^{\infty}\frac{\tilde{\phi}_n\big|_{r=R_i}}{\alpha_n}sin(\alpha_n x)\right)^2\right) \tag{24}$$

Simplifying assumption.

If the dynamic pressure drop (last term in Eq. (24)) is considered negligible, the vapour pressure profile becomes linear and can therefore be written as a Fourier serie where the pressure harmonics are linked to the heat flux harmonics at $r = R_i$ by:

$$\tilde{P}_{v,n} = \frac{-8\mu_v}{\pi\rho_v h_{lv} R_i^4}\left(\frac{1}{\alpha_n^2} + \frac{R_i^2}{8}\right)\tilde{\phi}_n\big|_{r=R_i} \tag{25}$$

Thanks to the linearisation of the saturation curve (13), heat flux and temperature harmonics at $r = R_i$ are then linked by:

$$\tilde{\phi}_n\big|_{r=R_i} = \frac{-K_{sat}}{\frac{8\mu_v}{\pi\rho_v h_{lv} R_i^4}\left(\frac{1}{\alpha_n^2} + \frac{R_i^2}{8}\right)}\,\tilde{\theta}_n\big|_{r=R_i} = -K_n\,\tilde{\theta}_n\big|_{r=R_i} \tag{26}$$

3.3.2. Liquid flow

Velocity profile.

In the same way as the vapour flow, the global mass balance of the liquid flow can be written:

$$\frac{du_l}{dx} = \frac{\phi\big|_{r=R_i}}{\rho_l A_w h_{lv}} \tag{27}$$

with $A_w = \pi(R_w^2 - R_i^2)$ the liquid section, and u_l the mean liquid velocity defined by:

$$u_l(x) = \frac{2}{R_w^2 - R_i^2}\int_{R_i}^{R_w} r\,u_x\,dr \tag{28}$$

Integrating Eq. (27) between 0 and x gives:

$$u_l(x) = \frac{2}{\rho_l A_w h_{lv} L}\sum_{n=1}^{\infty}\frac{\tilde{\phi}_n\big|_{r=R_i}}{\alpha_n} sin(\alpha_n x) \tag{29}$$

Pressure profile.

Liquid pressure drop in the porous wick is supposed to follow the Darcy law. Neglecting the dynamic pressure, the global momentum balance of the liquid flow is:

$$\frac{dP_l}{dx} = -\frac{\mu_l}{k_w}u_l + \rho_l g sin(\gamma) \tag{30}$$

Integrating Eq. (30) between 0 and x, and then assuming that the minimum capillary pressure (corresponding to the minimum of the difference $\Delta P_v(x) - \Delta P_l(x)$) is null (flat interface) and located at $x = x_0$, the expression of the liquid pressure can be written as:

$$P_l(x) = P_v(x_0) + \frac{2\mu_l}{\rho_l k_w A_w h_{lv} L}\sum_{n=1}^{\infty}\frac{\tilde{\phi}_n\big|_{r=R_i}}{\alpha_n^2}(cos(\alpha_n x) - cos(\alpha_n x_0)) + \rho_l g sin(\gamma)(x - x_0) \tag{31}$$

where $P_v(x_0)$ is evaluated directly from Eq. (24).

3.3.3. Capillary pressure

In the general case, the capillary pressure is just determined from the general expressions of the vapour and liquid pressures (Eqs (24) and (31)):

$$P_{cap}(x) = P_v(x) - P_l(x) \tag{32}$$

If the dynamic vapour pressure and the effects of the variation of the mean vapour velocity are considered negligible, with the evaporator and the condenser at each side of the heat pipe (standard configuration), the minimum capillary pressure is located at $x_0 = L$ and the maximum capillary pressure at $x = 0$. In this case, this maximum capillary pressure can be simply written:

$$P_{cap,max} = \rho_l g sin(\gamma) L - \frac{4}{L}\left[\frac{8\mu_v}{\pi\rho_v h_{lv} R_i^4} + \frac{\mu_l}{\rho_l k_w A_w h_{lv}}\right]\sum_{m=0}^{\infty}\frac{\tilde{\phi}_{2m+1}\big|_{r=R_i}}{\alpha_{2m+1}^2} \tag{33}$$

3.4. Calculation method

3.4.1. Quadrupole model used according to the model assumptions

From the previous development, the thermal quadrupole model can be more or less simplified according to the assumptions made on the effects of the temperature axial variation on heat transfer, and of taking into account the dynamic vapour pressure drop.

Whatever the assumptions, the fundamental ($n = 0$) of the quadrupole model gives:

$$\tilde{\theta}_0\big|_{r=R_o} = 0 \tag{34a}$$

$$\tilde{\phi}_0\big|_{r=R_o} = 0 \tag{34b}$$

The first equation corresponds to the equality between the two mean temperatures at $r = R_i$ and $r = R_o$. The second equation explicits a null global heat balance for the heat pipe.

With regard to the thermal harmonics, the different assumptions lead to more or less simple models:

- if the saturation temperature is considered uniform to estimate heat transfer, the quadrupole model is simplified by:

$$\begin{pmatrix} \tilde{\theta}_n \\ \tilde{\phi}_n \end{pmatrix}_{r=R_o} = \begin{pmatrix} \mathbb{A}_n & \mathbb{B}_n \\ \mathbb{C}_n & \mathbb{D}_n \end{pmatrix} \begin{pmatrix} 0 \\ \tilde{\phi}_n \end{pmatrix}_{r=R_i} \tag{35}$$

  This model is then decoupled from the hydrodynamic model. Both models can so be used independently of each other. From this quadrupole model, the harmonics of temperature and heat flux at $r = R_o$ can be directly linked:

$$\tilde{\phi}_n\big|_{r=R_o} = \frac{\mathbb{D}_n}{\mathbb{B}_n}\, \tilde{\theta}_n\big|_{r=R_o} \tag{36}$$

- if the thermohydraulic coupling is taken into account at the liquid/vapour interface :

  – in the case that dynamic vapour pressure drop is neglected, the thermodynamic coupling is linear (thanks to the linearisation of the saturation curve). The thermal quadrupole model can be written under the form:

$$\begin{pmatrix} \tilde{\theta}_n \\ \tilde{\phi}_n \end{pmatrix}_{r=R_o} = \begin{pmatrix} \mathscr{A}_n & \mathscr{B}_n \\ \mathscr{C}_n & \mathscr{D}_n \end{pmatrix} \begin{pmatrix} \tilde{\theta}_n \\ 0 \end{pmatrix}_{r=R_i} \tag{37}$$

  where the modified quadrupole coefficients are defined by:

$$\begin{pmatrix} \mathscr{A}_n & \mathscr{B}_n \\ \mathscr{C}_n & \mathscr{D}_n \end{pmatrix} = \begin{pmatrix} \mathbb{A}_n & \mathbb{B}_n \\ \mathbb{C}_n & \mathbb{D}_n \end{pmatrix} \begin{pmatrix} 1 & 0 \\ -K_n & 1 \end{pmatrix} \tag{38}$$

  with K_n defined in Eq. (26).

  From this modified quadrupole model, we can write then the direct relationship:

$$\tilde{\phi}_n\big|_{r=R_o} = \frac{\mathscr{C}_n}{\mathscr{A}_n}\, \tilde{\theta}_n\big|_{r=R_o} \tag{39}$$

  – if no vapour pressure drops are neglected, the initial quadrupole model (10) is used.

3.4.2. Estimation of temperature and heat flux fields

Solving the considered thermal quadrupole model from the external conditions of the heat pipe (see next section) provides the expressions (or calculations) of the integral transforms of θ and ϕ at the outer wall of the heat pipe ($r = R_o$). The integral transforms at $r = R_i$ are easily deduced from the global quadrupole model. From there, the integral transforms can be evaluated for any radius r thanks to the thermal quadrupole of each layer (Eq. 9), with a reference : for the wall layer the results at $r = R_o$, and for the porous layer the results at $r = R_i$. Finally, the temperature and heat flux fields can be calculated for all x and r by the inverse transform (Eq. 6), knowing that the fundamental transforms ($n = 0$) are null according to the developed model.

4. Model solution following external conditions

4.1. Solution with two heat flux sources

4.1.1. Problem description

The external boundary conditions can be simplified (Fig. 2) at first, with some assumptions:

- heat fluxes at both boundaries (evaporator and condenser) are imposed, with respective values q_E and q_C; this assumption is perfectly correct for the evaporator but it can be questionable for the condenser, for example if its size is not small compared to the size of the heat pipe ; both heat fluxes can be considered non-uniform on their respective length ; finally, the two heat fluxes can be considered as a single heat source, noted q, defined on the entire length of the heat pipe and equal to $-q_E$ at the evaporator, equal to q_C at the condenser and equal to zero along the adiabatic zone ;
- the heat losses with ambience are considered over the entire length of the heat pipe.

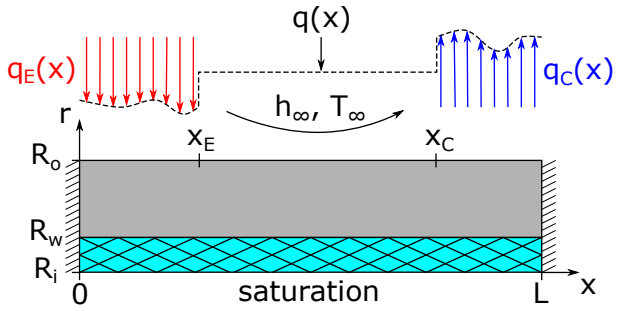

Figure 2: Simplified model of the cylindrical heat pipe with two heat flux sources

The integral tranforms of the heat flux at $r = R_o$ can be directly evaluated here:

$$\tilde{\phi}_0\big|_{r=R_o} = \tilde{q}_0 + 2\pi R_o h_\infty \, \tilde{\theta}_0\big|_{r=R_o} + 2\pi R_o h_\infty L(\overline{T}_{sat} - T_\infty) \tag{40a}$$

$$\tilde{\phi}_n\big|_{r=R_o} = \tilde{q}_n + 2\pi R_o h_\infty \, \tilde{\theta}_n\big|_{r=R_o} \tag{40b}$$

4.1.2. Solution of the quadrupole model

Eqs. (34a) and (34b), coupled with the expression (40a), provide the expression of $\overline{T}_{sat}$:

$$\overline{T}_{sat} = T_\infty - \frac{\tilde{q}_0}{2\pi R_o h_\infty L} \tag{41}$$

From this expression, it can be noticed that this mean saturation temperature can be only calculated if heat losses are defined ($h_\infty \neq 0$). If it is not the case, the value of $\overline{T}_{sat}$ must be provided with this model.

Direct analytical solution achievable.

If the saturation temperature is considered uniform in the estimation of heat transfer, Eqs. (36) and (40b) provide the expressions of the harmonics at $r = R_o$:

$$\tilde{\theta}_n\big|_{r=R_o} = \frac{\mathbb{B}_n}{\mathbb{D}_n - 2\pi R_o h_\infty \mathbb{B}_n} \tilde{q}_n \tag{42a}$$

$$\tilde{\phi}_n\big|_{r=R_o} = \frac{\mathbb{D}_n}{\mathbb{D}_n - 2\pi R_o h_\infty \mathbb{B}_n} \tilde{q}_n \tag{42b}$$

If the thermohydraulic coupling is considered with linear vapour pressure drop, from Eqs (39) and (40b), these equations turn into:

$$\tilde{\theta}_n\big|_{r=R_o} = \frac{\mathscr{A}_n}{\mathscr{C}_n - 2\pi R_o h_\infty \mathscr{A}_n}\tilde{q}_n \tag{43a}$$

$$\tilde{\phi}_n\big|_{r=R_o} = \frac{\mathscr{C}_n}{\mathscr{C}_n - 2\pi R_o h_\infty \mathscr{A}_n}\tilde{q}_n \tag{43b}$$

With both above first assumptions, if in addition the heat fluxes at evaporator and at the condenseur are uniform, the integral transforms of the heat source q can be easily evaluated. The temperature and the heat flux fields can be explicitly evaluated from the two total sources Q_E and Q_C, under the form:

$$\begin{pmatrix}\theta\\ \phi\end{pmatrix}_{x,r} = \begin{pmatrix}Z_E & Z_C\\ W_E & W_C\end{pmatrix}_{x,r}\begin{pmatrix}Q_E\\ -Q_C\end{pmatrix} \tag{44}$$

The impedances Z and the transmittances W are independent of the values of the imposed heat fluxes. So they are intrinsic properties of the heat pipe, depending on the fluid and material properties and on the location of the boundary conditions. Their expressions, with a thermohydraulic coupling, are for $J \in \{E, C\}$ (in parentheses, the references R_1 and R_2 for the coefficients of Table 1):

- for the porous wick layer ($R_1 = R_i$ and $R_2 = r$, where $R_i \le r \le R_w$):

$$Z_J\big|_{x,r} = \frac{2}{L}\sum_{n=1}^{\infty}\frac{A_n - B_n K_n}{2\pi R_o h_\infty \mathscr{A}_n - \mathscr{C}_n}\frac{\tilde{\chi}_{J,n}}{\tilde{\chi}_{J,0}}cos(\alpha_n x) \tag{45a}$$

$$W_J\big|_{x,r} = \frac{2}{L}\sum_{n=1}^{\infty}\frac{C_n - D_n K_n}{2\pi R_o h_\infty \mathscr{A}_n - \mathscr{C}_n}\frac{\tilde{\chi}_{J,n}}{\tilde{\chi}_{J,0}}cos(\alpha_n x) \tag{45b}$$

- for the wall layer ($R_1 = R_o$ and $R_2 = r$, where $R_w \le r \le R_o$):

$$Z_J\big|_{x,r} = \frac{2}{L}\sum_{n=1}^{\infty}\frac{A_n \mathscr{A}_n + B_n \mathscr{C}_n}{2\pi R_o h_\infty \mathscr{A}_n - \mathscr{C}_n}\frac{\tilde{\chi}_{J,n}}{\tilde{\chi}_{J,0}}cos(\alpha_n x) \tag{46a}$$

$$W_J\big|_{x,r} = \frac{2}{L}\sum_{n=1}^{\infty}\frac{C_n \mathscr{A}_n + D_n \mathscr{C}_n}{2\pi R_o h_\infty \mathscr{A}_n - \mathscr{C}_n}\frac{\tilde{\chi}_{J,n}}{\tilde{\chi}_{J,0}}cos(\alpha_n x) \tag{46b}$$

The $\chi_J(x)$ functions are the indicator functions, equal to 1 if x is in the considered domain (referenced by subscript J) and equal to 0 everywhere else.

Finally, the reference temperature $\overline{T}_{sat}$ is, from Eq. (41):

$$\overline{T}_{sat} = T_\infty + \frac{Q_E - Q_C}{2\pi R_o h_\infty L} \tag{47}$$

From this last equation, the temperature and heat flux fields can be rather expressed as a function of the arithmetic average of the source at evaporator and the source at condenser, $(Q_E + Q_C)/2$, and of the temperature difference $\overline{T}_{sat} - T_\infty$:

$$\begin{pmatrix}\theta\\ \phi\end{pmatrix}_{x,r} = \begin{pmatrix}Z & W_{sat}\\ W & Y_{sat}\end{pmatrix}_{x,r}\begin{pmatrix}\frac{Q_E+Q_C}{2}\\ \overline{T}_{sat} - T_\infty\end{pmatrix} \tag{48}$$

with the relationships: $Z = Z_E - Z_C$, $W = W_E - W_C$, $W_{sat} = \pi R_o h_\infty L(Z_E + Z_C)$ and $Y_{sat} = \pi R_o h_\infty L(W_E + W_C)$.

If no heat loss is taken into account ($h_\infty = 0$), no more link exits between saturation temperature and heat sources. The mean saturation temperature has to be imposed and the last relation can not be written. However, in that case, the heat fluxes at evaporator and condenser are necessarily equal: $Q_E = Q_C = Q$. Eq. (44) is then simply written as:

$$\begin{pmatrix}\theta\\ \phi\end{pmatrix}_{x,r} = \begin{pmatrix}Z\\ W\end{pmatrix}_{x,r} Q \tag{49}$$

The previously defined transmittance W_{sat} and the admittance Y_{sat} characterise thus the effects of heat losses with ambience for a given temperature difference $\overline{T}_{sat} - T_\infty$.

With regard to the capillary pressure, in the case of uniform heat fluxes at evaporator and at condenser, located at each extremity of the heat pipe, and with Darcy-Weisbach vapour pressure drop only, the following explicit expression of the maximum capillary pressure is obtained from Eq. (33), all calculations done (with a thermohydraulic coupling):

$$P_{cap,max} = \rho_l g sin(\gamma) L - \frac{4L}{\pi^3 L_{\text{eff}}} \left(\frac{8\mu_v L_{\text{eff}}}{\pi \rho_v h_{lv} R_i^4} + \frac{\mu_l L_{\text{eff}}}{\rho_l A_w h_{lv} k_w} \right) \sum_{J \in E,C} Q_J \frac{L_J}{L} \sum_{m=0}^{\infty} \frac{-K_{2m+1}}{2\pi R_o h_\infty \mathscr{A}_{2m+1} - \mathscr{C}_{2m+1}} \frac{sin(\alpha_{2m+1} L_J)}{(2m+1)^3} \tag{50}$$

with $L_{\text{eff}} = L - 0.5(L_E + L_C)$, the effective length of the heat pipe.

Moreover, if the heat pipe is perfectly insulated, it can be assumed that $h_\infty = 0$ and the heat power Q is the same at evaporator and at condenser. The following expression of the heat pipe capillary limit can be deduced:

$$Q_{cap,max} = \frac{\frac{2\sigma}{R_{\text{eff}}} - \rho_l g sin(\gamma) L}{\frac{8\mu_v L_{\text{eff}}}{\pi \rho_v h_{lv} R_i^4} + \frac{\mu_l L_{\text{eff}}}{\rho_l k_w A_w h_{lv}}} \frac{\frac{\pi^3 L_{\text{eff}}}{4L}}{\sum_{J \in \{E,C\}} \sum_{m=0}^{\infty} \frac{\frac{L}{L_J} sin\left(\frac{(2m+1)\pi L_J}{L}\right)}{(2m+1)^3} \frac{-K_{2m+1}}{\mathscr{C}_{2m+1}}} \tag{51}$$

with R_{eff} the effective pore radius of the wick.

This expression is similar to the analytical expression given by Lips and Lefèvre [8]. The first factor in the product corresponds to the well-known analytical expression of the capillary limit when the heat conduction in the wall and in the porous wick is neglected [2]. The second term is a correction factor taking into account this phenomenon. This term is always greater than 1. It has to be noticed that, when the solid structure is neglected, coefficients $\mathscr{C}_n$ tend to $-K_n$, and so the correction factor is well equal to 1:

$$\frac{\frac{\pi^3 L_{\text{eff}}}{4L}}{\sum_{J \in \{E,C\}} \sum_{m=0}^{\infty} \frac{\frac{L}{L_J} sin\left(\frac{(2m+1)\pi L_J}{L}\right)}{(2m+1)^3}} = 1 \tag{52}$$

Finally, still in the case of the simplified model with uniform heat fluxes at evaporator and at condenser, intrinsic relationships can be developed between each hydrodynamic variables (pressure or velocity) and the heat flux inputs, as well as for the thermal variables (with impedances and transmittances).

Iterative analytical solving required.

If no assumption is made (thermohydraulic coupling and nonlinear vapour pressure drop), a direct analytical solution is not possible. An iterative procedure is thus necessary.

On the one hand, from the quadrupole model (10) and Eq. (40b), the following linear relation can be written:

$$\tilde{\phi}_n\big|_{r=R_i} = \frac{\tilde{q}_n - (\mathbb{C}_n - 2\pi R_o h_\infty \mathbb{A}_n)\, \tilde{\theta}_n\big|_{r=R_i}}{\mathbb{D}_n - 2\pi R_o h_\infty \mathbb{B}_n} \tag{53}$$

On the other hand, the linearisation of the saturation curve (14) and the expression of the vapour pressure (24) provides the expression for $\theta|_{r=R_i}$ as a function of the harmonics of $\phi\big|_{r=R_i}$. From the definition of the integral transform (5), the following equation is finally obtained:

$$\tilde{\theta}_n\big|_{r=R_i} = -\frac{8\mu_v}{\pi \rho_v h_{lv} R_i^4 K_{sat}} \left(\frac{1}{\alpha_n^2} + \frac{R_i^2}{8} \right) \tilde{\phi}_n\big|_{r=R_i} - \frac{4}{3\pi^2 \rho_v h_{lv}^2 R_i^4 L K_{sat}} \left(2 \sum_{m=1}^{\infty} \frac{\tilde{\phi}_m\big|_{r=R_i}\, \tilde{\phi}_{m+n}\big|_{r=R_i}}{\alpha_m \alpha_{m+n}} - \sum_{m=1}^{n-1} \frac{\tilde{\phi}_m\big|_{r=R_i}\, \tilde{\phi}_{n-m}\big|_{r=R_i}}{\alpha_m \alpha_{n-m}} \right) \tag{54}$$

The very fast iterative procedure between the two above equations provides the harmonics of temperature and heat flux at $r = R_i$. The quadrupole model allows to go back to the values of the harmonics at $r = R_o$.

4.2. Solving with one heat flux source and one temperature source

Under real conditions, described in section 2, the problem can not be solved directly by thermal quadrupoles anymore, because the external conditions are localised at specific lengths of the heat pipe (Fig. 3).

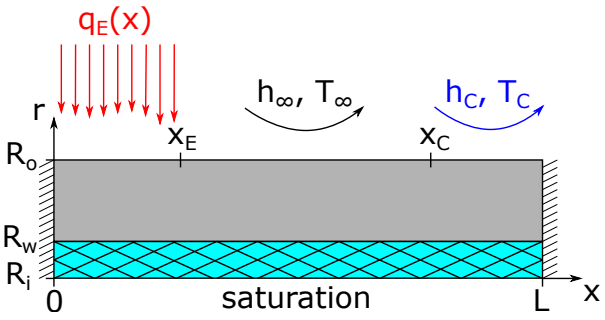

Figure 3: Model of the cylindrical heat pipe with one heat flux source and one temperature source

The idea is here to mesh the external wall following the direction x, with points $x_{i,1\leq i\leq N} \in [0;L]$ and to find the unknown variables (temperature and/or heat fluxes) on this side of the heat pipe. To simplify the notation, the mentioned variables in the original domain (depending on x and r) are at $r = R_o$ in the rest of this paragraph.

On the one hand, the heat flux at $r = R_o$ can be written:

$$\phi(x) = -\chi_E(x)q_E(x) + \chi_A(x)2\pi R_o h_\infty(T(x) - T_\infty) + \chi_C(x)2\pi R_o h_C(T(x) - T_C) \tag{55}$$

On the other hand, from the quadrupole model (10) and for any case, this heat flux can be written:

$$\phi(x) = \frac{2}{L}\sum_{n=1}^{\infty}\frac{\mathbb{D}_n}{\mathbb{B}_n}\tilde{\theta}_n\big|_{r=R_o} cos(\alpha_n x) - \frac{2}{L}\sum_{n=1}^{\infty}\frac{1}{\mathbb{B}_n}\tilde{\theta}_n\big|_{r=R_i} cos(\alpha_n x) \tag{56}$$

If uniform saturation temperature is supposed in the thermal model (with any kind of vapour pressure drop) or if a thermohydraulic coupling is considered with linear vapour pressure drop, Eq (56) can be simplified with only the harmonics $\tilde{\theta}_n\big|_{r=R_o}$ (Appendix A). In any case, the expressions of these harmonics are developed as function of the external temperatures from Eq (5) by a standard Newton-Cotes method.

Equality of Eqs. (55) and (56) is then written for all x_i of the mesh. For both cases of uniform $\overline{T}_{sat}$ for the thermal model and of thermohydraulic coupling with linear ΔP_v, it leads to a linear system under the form $AX = BU$ (Appendix A), linking the unknown variables X, namely the temperatures $T(x_i)$, and the inputs U, namely $q_E(x_i)$, T_∞ and T_C. An iterative procedure is nevertheless necessary to solve this system by introducing a closure equation to evaluate $\overline{T}_{sat}$ on which matrix A depends (Fig. A.1).

For the case of a thermohydraulic coupling with nonlinear vapour pressure drop, a more complex iterative procedure is necessary (Fig. A.2), involving in particular the nonlinear expression of $\tilde{\theta}_n\big|_{r=R_i}$ (Eq. (54)). It leads to a system under the form $AX = BU + C$, with C is a vector taking into account the nonlinearities at the liquid/vapour interface (Appendix A).

Once the system is solved, the integral transforms of temperature at $r = R_o$ are deduced from the discretisation:

$$\tilde{\theta}_n\big|_{r=R_o} = \sum_{j=1}^{N} w_j(T(x_j) - \overline{T}_{sat})cos(\alpha_n x_j) \tag{57}$$

with w_j the coefficients of the Newton-Cotes method.

Then, the quadrupole model will provide temperature and heat flux fields (see section 3.4.2).

4.3. Summary

The different ways to solve both models (according to the external thermal conditions) for the three assumptions introduced at the liquid/vapour interface are summarised in Table 2 as a synthesis of the introduced mathematical developments.

External thermal conditions	**Uniform T_v for thermal model** **Any ΔP_v**	**Thermohydraulic coupling at the interface** **Linear ΔP_v**	**Thermohydraulic coupling at the interface** **Nonlinear ΔP_v**
Two heat flux sources*	Direct analytical expressions of thermal harmonics		Iterative solving for inner thermal harmonics
Heat flux source + Temperature source	Iterative solving for (x,r) depending external thermal variables		Iterative solving for (x,r) depending external thermal variables and for inner thermal harmonics
*in the case of imposed heat flux sources and with no ambient losses, the value of $\overline{T}_{sat}$ is required			

Table 2: Solving summary of the model according to external conditions and saturation thermohydraulic coupling

It can be noticed that iterative procedures are very fast with respect to other numerical methods, even in the worst case (less than five minutes with a standard computer for the case of a thermohydraulic coupling with nonlinear vapour pressure drop).

5. Comparison between model and literature results

To confirm the results of the developed model, they are compared with two different cases from Shabgard and Faghri studies [7] on copper/water heat pipes. The first case, named case A, corresponds to a standard heat pipe, with evaporator and condenser at each extremity, without heat losses and with a convective cooling boundary condition at the condenser. The second case, named case B, is a heat pipe subjected to four evaporators and one condenser with conditions of imposed heat fluxes, still without heat losses. The main specifications of both cases are given in Table 3.

While case A is compared directly to the model with one heat flux and one temperature sources (section 4.2), case B is compared to the model with imposed heat fluxes (section 4.1.2). The different conditions at the liquid/vapour interface are studied for both cases.

5.1. Single uniform heat source and convective cooling

For case A, the mean saturation temperature calculated by the model is in particular evaluated from boundary conditions. The axial temperatures are plotted in Fig. 4a. The axial capillary pressure and vapour velocity are compared in Fig. 4b. It appears that the influence either of the thermohydraulic coupling or of the vapour pressure drop on these variables is not very significant. The presented profiles are thus quite similar regardless of these conditions.

External wall temperatures fit almost perfectly. It can be noticed that the mean saturation temperature matches to the temperature in the adiabatic zone very well, even if the thermal gradient in this zone is the strongest.

The capillary pressure and vapour velocity profiles are likewise well reproduced. It can be noticed in that case, that the capillary pressure mainly balances the liquid pressure drop. The evolution of the mean vapour velocity is standard with an increase along the evaporator, a maximum in the adiabatic zone and a decrease along the condenser.

To complete this study, it is interesting to analyse the evolution of the vapour pressure according to the modelling assumptions (Fig. 5). Even if the vapour pressure drop is of the order of a dozen pascals, the nonlinear

Specification	**Case A**	**Case B**
Working fluid	Water	Water
Wall material	Copper	Copper
Wick material	Copper	Copper
Total length	0.89 m	1 m
Number of heater(s)	1	4
Location of heater(s)	[0, 0.6] m	[0.02, 0.0835] m [0.159, 0.222] m [0.298, 0.361] m [0.436, 0.500] m
Location of condenser	[0.69, 0.89] m	[0.68, 0.98] m
Inner radius	7.9 mm	10.29 mm
Wall thickness	0.9 mm	1.7 mm
Wick thickness	0.75 mm	0.71 mm
Wick porosity	0.9	0.7
Wick permeability	$1.5\ 10^{-9}$ m^2	$1.3\ 10^{-9}$ m^2
Wick effective thermal conductivity	1.97 W m^{-1} K^{-1}	1.16 W m^{-1} K^{-1}
Heat flux at evaporator(s)	455 W	50 W per heater
Boundary at condenser	Convective cooling h_C = 1800 W m^{-2} K^{-1} T_C = 26°C	Uniform cooling Q_C = 200 W T_{sat} = 71.4°C
Comparative model	Heat flux source + Temperature source	Two heat flux sources

Table 3: Main specifications of the two heat pipes from Shabgard and Faghri [7]

dynamic pressure drop is important to consider and are of the same order of magnitude as viscous pressure drop. Considering these latter, it can be noticed that the term depending on the acceleration of the vapour velocity (second term in Eq. (22)) is negligible compared to Darcy-Weisbach pressure drop. Taken all the pressure drops into account, the well-known phenomena of injection at the evaporator (due to the increase of the vapour velocity) and of suction at the condenser (due to the decrease of the velocity) are highlighted.

Finally, regardless of the losses considered, a shifting of the absolute value of the vapour pressure is noted if the thermohydraulic coupling at the liquid/vapour interface is considered. This difference comes simply from the evaluation of the mean saturation temperature corresponding to the mean external temperatures. From a zoom on the wall temperatures at the evaporator and the condenser (Fig. 6), a slight difference on the profiles is noted. It comes directly from the slight axial variation of the saturation temperature. With any vapour pressure drop, the thermohydraulic coupling implies a small change of $\overline{T}_{sat}$ and so of the reference vapour pressure.

5.2. Multiple uniform heat sources and uniform cooling

For case B, equal multi-sources are directly applied at four different evaporators and the cooling is also considered uniform. However, no heat losses are considered, which implies that no reference temperature exists and the mean saturation temperature has to be provided for the model as previously mentioned. As for case A, axial temperatures, and axial capillary pressure and vapour velocity, are plotted, respectively, in Fig. 7a and 7b.

Results of literature and the simulations match perfectly. The increases and decreases of temperature at and between evaporators are well determined. Here the mean saturation temperature corresponds to the temperature in the main adiabatic zone (between evaporators and condenser). While capillary pressure evolution is similar to case A with one heat source, the impact of the multi-sources is well highlighted by the distribution of the vapour velocity, with a more or less high increase following the evaporators and the adiabatic zones. The impact of the dynamic pressure drop on the vapour pressure is the same as for case A, but the thermohydraulic coupling has no

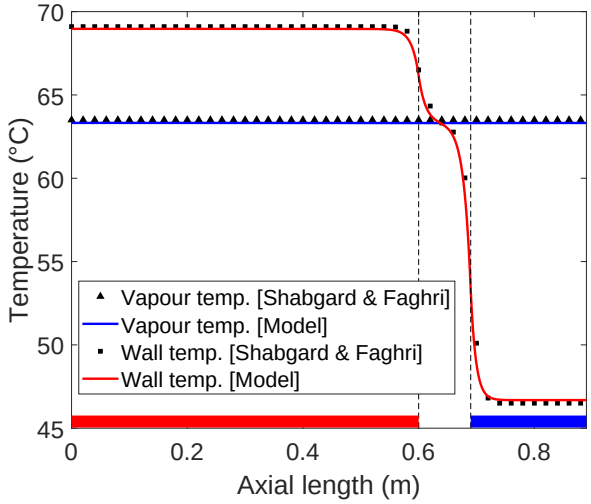

(a) Axial temperatures

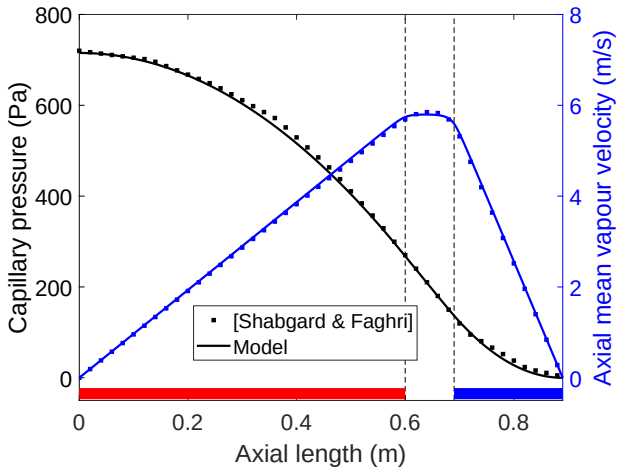

(b) Axial capillary pressure and mean vapour velocity

Figure 4: Case A - Comparison with results from Shabgard and Faghri [7]

more effects because $\overline{T}_{sat}$ is imposed.

As mentioned in section 4.1.2, the behaviour of the heat pipe in this example can be intrinsically characterised by impedances and transmittances. For example, the temperature field can be deduced from the transferred heat flux and the impedance of the system, illustrated in Fig. 8, by $T|_{x,r} = \overline{T}_{sat} + Z|_{x,r}\, Q$ (from Eq. (49)). This thermal impedance is completely independent of the total imposed heat flux Q. In Fig. 8, it can be observed that this impedance is strongly linked to the locations of the evaporators and the condenser, especially in the wall of the heat pipe. Its value becomes more and more homogeneous along the axial length within the porous, until a zero value at the liquid/vapour interface. It means that, for an imposed saturation temperature, when the heat flux increases, the axial temperature gradient increases more in the wall than in the porous wick. Finally, in the main adiabatic zone, its value is also close to zero over most of the area, both in the porous wick and in the wall.

For the same case with heat losses, with for example $h_\infty = 10\ \mathrm{W.m^{-2}.K^{-1}}$, the thermal impedance field is quite similar to the previous one in Fig. 8 with a maximal variation of $2.5\ 10^{-4}\ \mathrm{K.W^{-1}}$. The transmittance W_{sat} field,

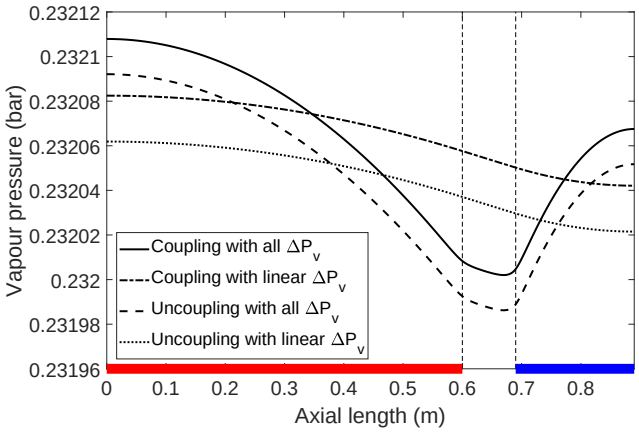

Figure 5: Case A - Vapour pressure depending on model assumptions

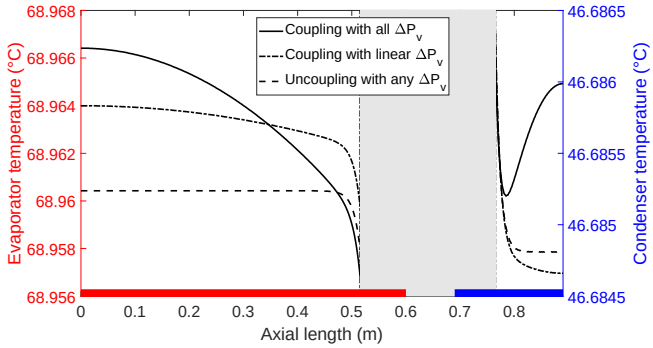

Figure 6: Case A - Zoom on wall temperatures at evaporator and condenser depending on model assumptions

defined in Eq. (48), is highlighted in Fig. 9. This transmittance is positive in evaporators and condenser, and negative in the adiabatic zones. It means that, for a fixed ambience temperature and at fixed mean heat flux, if the saturation temperature $\overline{T}_{sat}$ increases, the difference between $\overline{T}_{sat}$ and the temperatures at evaporators and at condenser increases, while the temperatures in adiabatic zones get closer to $\overline{T}_{sat}$. It implies an increase of the axial thermal gradients. It can be noticed that this impact affects both temperature fields in the wall and in the porous wick, even if it is attenuated in the latter. Finally, it is verified that this transmittance W_{sat} is near zero at the liquid/vapour interface, as well as the impedance Z, which indicates a quasi uniformity of the saturation temperature along the axial direction.

6. Significance of the thermohydraulic coupling

After the previous validation of the model, an analysis is finally proposed to study a case where the influence of the non-uniformity of the saturation temperature along the length of the heat pipe affects substantially its thermohydraulic behaviour. The fixed geometrical specifications and boundary conditions of the studied case are gathered in Table 4. The standard problem of a heat pipe under realistic boundary conditions (model with heat source and one temperature source), with evaporator and condenser at each extremety is considered. The chosen heat pipe is especially small in diameter and the heat flux imposed at evaporator is relatively low (small mean saturation temperature). Due to the effects of the thermohydraulic coupling on the evaluation of $\overline{T}_{sat}$ (see section 5.1), the imposed heat flux at evaporator is adapted to have nearly the same $\overline{T}_{sat}$ in both cases ($Q_E = 4.7$ W with thermohydraulic coupling and $Q_E = 5.2$ W without).

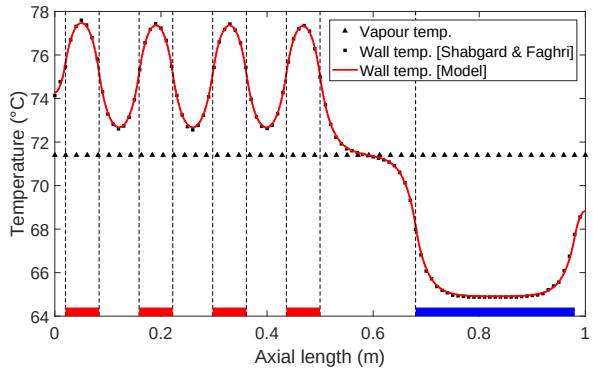

(a) Axial temperatures

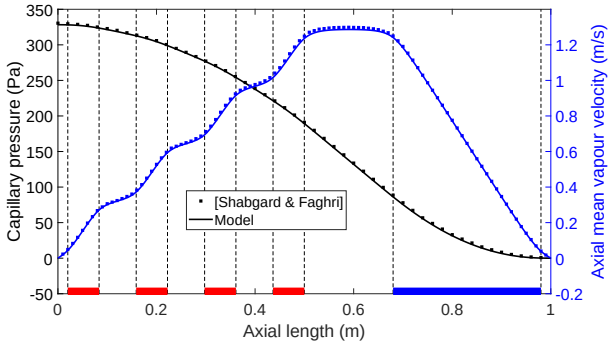

(b) Axial capillary pressure and mean vapour velocity

Figure 7: Case B - Comparison with results from Shabgard and Faghri [7]

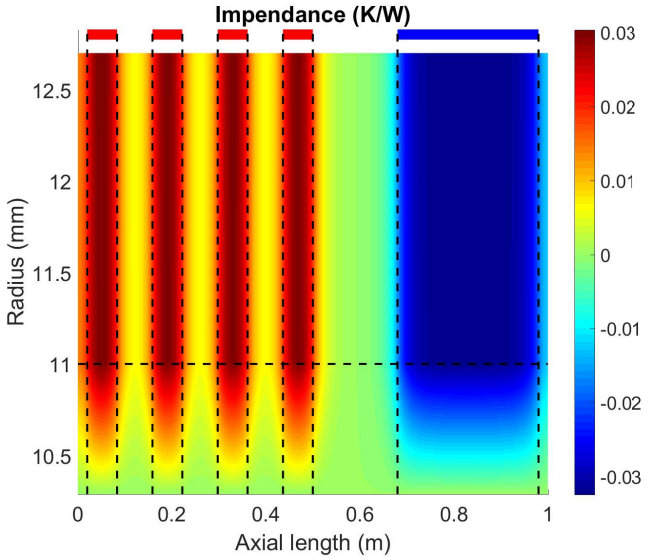

Figure 8: Case B - Thermal impedance field (Z from Eq. (49)) of θ from the total heat source Q

The temperature and pressure profiles are illustrated in Fig. 10. A variation of more than 2.5°C is present for

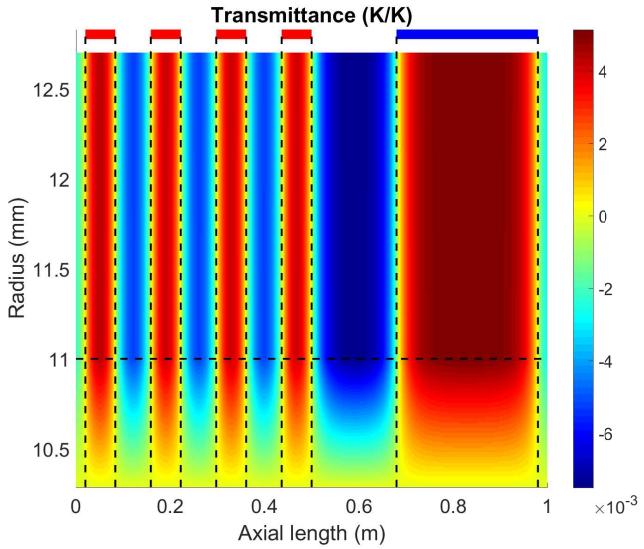

Figure 9: Case B with additional heat losses (h_∞ = 10 W.m^{-2}.K^{-1}) - Thermal transmittance field (W_{sat} from Eq. (48)) of θ from the temperature difference $\overline{T}_{sat} - T_\infty$

Working fluid	Water
Wall material	Copper
Wick material	Copper
Total length	1 m
Location of evaporator	[0, 0.3] m
Location of condenser	[0.7, 1] m
Inner radius	1.5 mm
Wall thickness	1 mm
Wick thickness	0.5 mm
Wick porosity	0.7
Wick permeability	1.5 10^{-9} m^2
Effective thermal conductivity of the wick	1 W m^{-1} K^{-1}
Mean saturation temperature	20°C
Convective cooling at condenser	h_C = 100 W m^{-2} K^{-1}
	T_C = 10°C

Table 4: Specifications of the heat pipe for the analysis

the saturation temperature around 20°C. It involves an increase of 1.2°C of the maximal temperature at evaporator and a decrease of 1.15°C of the minimal temperature at condenser, compared to the case without thermohydraulic coupling. It implies an increase of the lengthwise thermal gradient and a non-uniformity of temperatures in the adiabatic zone, equal to that of saturation. The consideration of the uniformity of the saturation temperature for the thermal model implies also a decrease of both liquid and vapour pressure drops, slightly more substantial for the vapour flow. It involves a 10% decrease of the maximal capillary pressure in that case. Compared to a standard heat pipe, it can be noticed that liquid and vapour pressure drops are of the same order of magnitude.

Finally, we can look in more details at the difference of temperature fields inside the wall and the porous of the heat pipe (Fig 11). With the thermohydraulic coupling, the lengthwise thermal gradient is conserved in the wall thickness while the thermal gradient in the porous media is more two-dimensional. With a considered uniform saturation temperature, the thermal gradient is mainly radial in the porous wick, while relatively constant temperatures are observed in each part of the wall of the heat pipe.

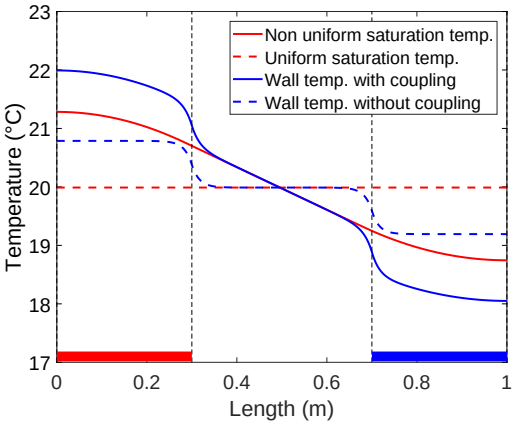

(a) Axial temperatures

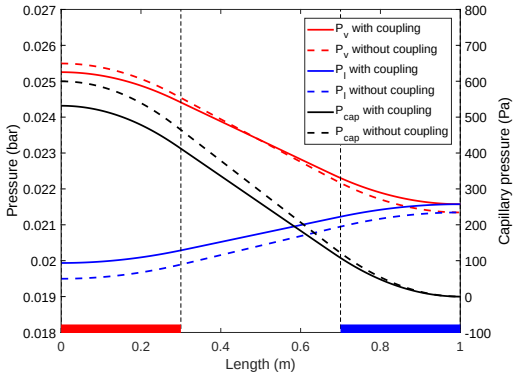

(b) Fluid pressures

Figure 10: Micro heat pipe with an operating temperature of 20°C

To conclude this section, it is to highlight that, in the studied conditions, the model with two heat flux sources with a uniform imposed heat flux at condenser gives similar results, whatever the coupling is taken into account. The only drawback of this simple model is that the variation of the mean saturation temperature with respect to the transferred heat flux has to be known if no heat losses with ambience are considered.

7. Conclusion

A generalisation of steady state analytical models of cylindrical heat pipe by Fourier integral transforms has been proposed in this article. By assuming axisymetric boundary conditions, two types of models have been developed via an original mathematical representation by thermal quadrupoles for the two-dimensional conductive heat transfer. A first simplified model with both imposed heat fluxes at evaporator and at condenser enables a direct analytical solution for heat transfer in the wall and in the porous wick and for the pressure drops in liquid and vapour flows, under specific thermodynamic conditions at the liquid/vapour interface. A second model with more realistic boundary conditions, especially a convective cooling at condenser, requires a mesh over the outer wall of the heat pipe and a fast iterative procedure. For either models, three kind of inner thermohydraulic conditions have been taken into account: a decoupling of thermal and hydraulic models, or a stronger coupling between heat transfer at the interface and the vapour pressure drop, considered either linear or nonlinear. It has been shown that the operating temperature of the heat pipe can be evaluated from boundary conditions in the

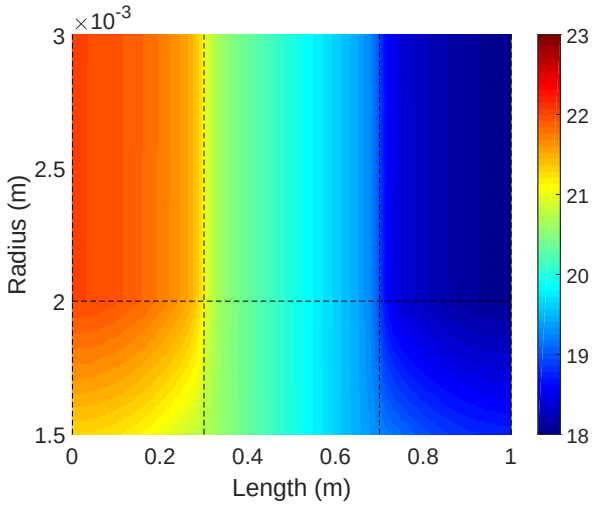

(a) With non uniform saturation temperature

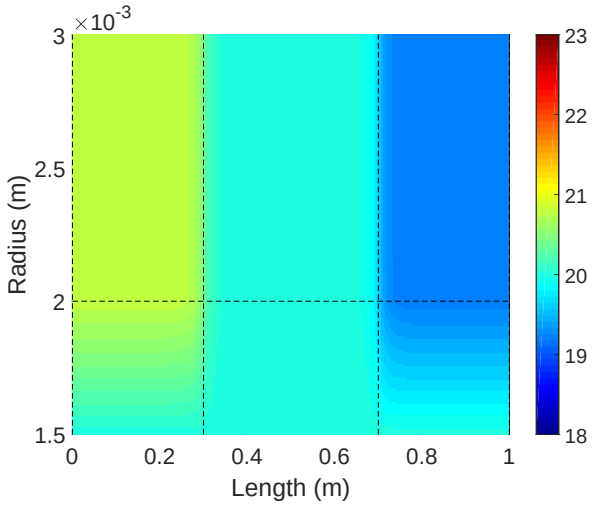

(b) With uniform saturation temperature

Figure 11: Temperature fields (°C) for micro heat pipe with an operating temperature of 20°C

case where some heat losses with ambience are taken into account. If no reference temperature exists in the problem definition, this operating temperature has to be provided additionally to solve analytically the heat transfer equations.

The model results have been validated by comparison with literature results in both cases with uniform or convective cooling at condenser, as well through temperature, capillary pressure and velocity distributions. An example with multiple sources at evaporator has been easily treated with this methodology.

In the case of uniform heat fluxes at evaporator and at condenser, an original determination of temperature and radial heat flux fields for imposed boundary conditions have been introduced, with the definition of thermal impedances, transmittances or admittances of the heat pipe. These latter are intrinsic properties of the heat pipe subject to any thermal sollicitations. They depend directly on fluid and material properties and on the location of the boundary conditions.

The introduced analyses have shown that the uniformity of saturation temperature can be considered to model a large diameter heat pipe, but not a micro heat pipe where strong vapour pressure drop and two-dimensional thermal gradients in the wick are present.

As well as previous analytical models proposed in literature, this model have some limits regarding some specific phenomena, as for example no thermal effect on the interface curvature or no possible inclusion of liquid slug at the condenser. However, as the previous models, the introduced model can be used to design a capillary cylindrical heat pipe or to be included more easily in an optimisation process than a complete numerical tool. Furthermore, the original quadrupoles representation suggests simpler developments of more complex models in three-dimensional or in transient regime, with an additional Laplace time integral transform. The development of analytical models for flat heat pipes can also be easily considered under the same formalism.

Nomenclature

Latin letters

A	section	m^2
g	gravitational acceleration	$m.s^{-2}$
h	heat transfer coefficient	$W.m^{-2}.K^{-1}$
h_{lv}	latent heat	$J.kg^{-1}$
k_w	permeability of porous wick	m^2
K_{sat}	linearisation coefficient of the saturation curve	$Pa.K^{-1}$
L	heat pipe length	m
N	number of mesh points	
P	pressure	Pa
q	heat flux	$W.m^{-1}$
Q	heat power	W
r	radius coordinate	m
R	radius	m
T	temperature	K or °C
u	velocity	$m.s^{-1}$
W	transmittance	
w_j	quadrature coefficients	m
x	length coordinate	m
Y	admittance	$W.K^{-1}$
Z	impedance	$K.W^{-1}$

Greek letters

α_n	eigenvalue of order n following x	m^{-1}
γ	angle of heat pipe with horizontal	
ϵ	porosity	
θ	temperature difference	K
λ	thermal conductivity	$W.m^{-1}.K^{-1}$
μ	dynamic viscosity	Pa.s
ρ	density	$kg.m^{-3}$
σ	surface tension	$N.m^{-1}$
ϕ	radial heat flux	$W.m^{-1}$
χ	indicator function	

Subscripts and superscripts

A	adiabatic zone
C	condenser
E	evaporator
eff	effective
eq	equivalent
i	inner radius
l	liquid
o	outer radius
r	radial
sat	saturation
v	vapour
w	porous wick
x	axial
∞	ambience

Appendix A. Setting up the system for the model with one heat flux source and one temperature source and iterative procedure

Appendix A.1. Linear system

If a uniform saturation temperature is supposed for the thermal model (with any vapour pressure drop) or if a thermohydraulic coupling is considered with linear vapour pressure drop, Eq. (56) can be simply written as:

$$\phi(x) = \frac{2}{L}\sum_{n=1}^{\infty} \mathscr{Y}_n \, \tilde{\theta}_n\big|_{r=R_o} cos(\alpha_n x) \tag{A.1}$$

with the admittance $\mathscr{Y}_n = \mathbb{D}_n/\mathbb{B}_n$ in the case where a uniform saturation temperature is assumed and $\mathscr{Y}_n = \mathscr{C}_n/\mathscr{A}_n$ with thermohydraulic coupling and linear vapour pressure drop.

In this equation, the integral transforms of temperature can be evaluated by a standard Newton-Cotes method, as trapezoidal rule, under the form:

$$\tilde{\theta}_n\big|_{r=R_o} = \int_0^L T(x')cos(\alpha_n x')dx' = \sum_{j=1}^{N} w_j \, T(x_j)cos(\alpha_n x_j) \tag{A.2}$$

From the equality of Eqs. (55) and (56), for all x_i of the mesh, a relationship of the following form is derived:

$$2\pi R_o[h_\infty \chi_A(x_i) + h_C\chi_C(x_i)]\,T(x_i) + \sum_{j=1}^{N} \omega_{ij}\,T(x_j) = \chi_E(x_i)q_E(x_i) + \chi_A(x_i)2\pi R_o h_\infty T_\infty + \chi_C(x_i)2\pi R_o h_C T_C \tag{A.3}$$

with the coefficients ω_{ij} defined as:

$$\omega_{ij} = -\frac{2}{L} w_j \sum_{n=1}^{\infty} \mathscr{Y}_n cos(\alpha_n x_i) cos(\alpha_n x_j) \tag{A.4}$$

Eq. (A.3) can be written under matrix form, for $1 \le i \le N$ and $1 \le j \le N$:

$$\left(\left(\omega_{ij}\right) + \begin{pmatrix} \mathbf{0}_{N_E} & \mathbf{0}_{N_E,N_A} & \mathbf{0}_{N_E,N_C} \\ \mathbf{0}_{N_A,N_E} & 2\pi R_o h_\infty \mathbf{I}_{N_E} & \mathbf{0}_{N_A,N_C} \\ \mathbf{0}_{N_C,N_E} & \mathbf{0}_{N_C,N_A} & 2\pi R_o h_C \mathbf{I}_{N_C} \end{pmatrix}\right)\left(T(x_j)\right) = \begin{pmatrix} \mathbf{I}_{N_E} & \mathbf{0}_{N_E,1} & \mathbf{0}_{N_E,1} \\ \mathbf{0}_{N_A,N_E} & 2\pi R_o h_\infty \mathbf{1}_{N_A,1} & \mathbf{0}_{N_A,1} \\ \mathbf{0}_{N_C,N_E} & \mathbf{0}_{N_C,1} & 2\pi R_o h_C \mathbf{1}_{N_C,1} \end{pmatrix}\begin{pmatrix} \left(q_E(x_i)\right) \\ T_\infty \\ T_C \end{pmatrix} \tag{A.5}$$

which can be written under the form $AX = BU$, with X the unknown external temperatures and U the heat and temperature sources.

Through the expressions of the quadrupole coefficients in the terms of ω_{ij} coefficients, matrix A depends on the unknown temperature $\overline{T}_{sat}$. So, an iterative procedure is necessary. The iterative closure equation to evaluate the new value of $\overline{T}_{sat}$ stems from Eq. (34a) by using the mesh:

$$\overline{T}_{sat} = \frac{1}{L}\sum_{j=1}^{N} w_j T(x_j) \tag{A.6}$$

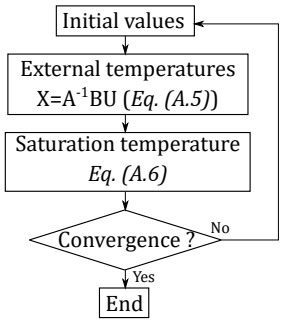

Figure A.1: Flowchart of the iterative procedure for solving linear system

If the assumption of a uniform saturation temperature is considered and if the liquid conductivity can be considered as independent of $\overline{T}_{sat}$, the same is true for matrix A. No more iterative procedure is necessary and the linear system (A.5) can be solved directly.

Appendix A.2. Nonlinear system

In the case of a thermohydraulic coupling with nonlinear vapour pressure drop, Eq. (56) can not be simplified any more. With a similar development as in the previous linear case, the equality of Eqs (55) and (56) leads to a system under the form $AX = BU + C$, with $\mathscr{Y}_n = \mathbb{D}_n/\mathbb{B}_n$ in matrix A while vector C is expressed as:

$$C_i = -\frac{2}{L}\sum_{n=1}^{\infty}\frac{1}{\mathbb{B}_n}\,\tilde{\theta}_n\big|_{r=R_i}\, cos(\alpha_n x_i) \tag{A.7}$$

In that case, each harmonic $\tilde{\theta}_n\big|_{r=R_i}$ can be expressed from Eq. (54) as nonlinear function of the harmonics $\tilde{\phi}_n\big|_{r=R_i}$. Furthermore, from the quadrupole model and the Newton-Cotes method, these latter harmonics can be expressed as:

$$\tilde{\phi}_n\big|_{r=R_i} = \sum_{j=1}^{N} w_j \left(\mathbb{A}_n \phi(x_j) - \mathbb{C}_n T(x_j)\right) cos(\alpha_n x_j) \tag{A.8}$$

where the heat fluxes $\phi(x_j)$ are evaluated from Eq (55) as function of the $T(x_j)$ variables (deduced by solving the matrix system).

The iterative procedure involves finally the closure equation for the evaluation of the new value of $\overline{T}_{sat}$ (Eq. (A.6)).

Appendix A.3. Comments

It can be noticed that some numerical precautions must be implemented for a good convergence of iterations. The main one is imposing the equality between the number of subintervals for the Newton-Cotes method $(N-1)$ and the number of harmonics for the calculation of the infinite sum. The purpose is to numerically preserve the orthogonality of the cosine functions.

The previous developments can be done for any kind of boundary conditions, especially at the condenser.

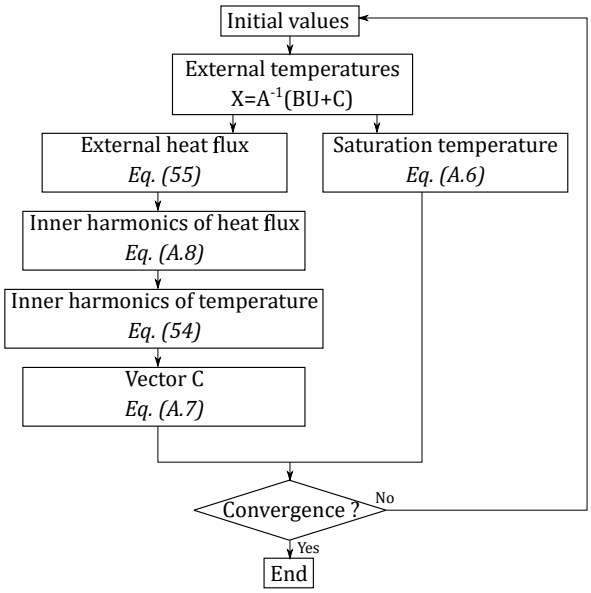

Figure A.2: Flowchart of the iterative procedure for solving nonlinear system

References

[1] N. Blet, S. Lips, and V. Sartre. Heats pipes for temperature homogenization : a literature review. *Applied Thermal Engineering*, 118:490–509, 2017.

[2] A. Faghri. *Heat Pipe Science and Technology*. Taylor and Francis, 1995.

[3] Z.J. Zuo and A. Faghri. A network thermodynamic analysis of the heat pipe. *International Journal of Heat and Mass Transfer*, 41:1473–1484, 1998.

[4] N. Zhu and K. Vafai. Analysis of cylindrical heat pipes incorporating the effects of liquid-vapor coupling and non-darcian transport - a closed form solution. *International Journal of Heat and Mass Transfer*, 42:3405–3418, 1999.

[5] S.J. Kim, J.K. Seo, and K.H. Do. Analytical and experimental investigation on the operational characteristics and the thermal optimization of a miniature heat pipe with a grooved wick structure. *International Journal of Heat and Mass Transfer*, 46:2051–2063, 2003.

[6] M. Aghvami and A. Faghri. Analysis of flat heat pipes with various heating and cooling configurations. *Applied Thermal Engineering*, 31:2645–2655, 2011.

[7] H. Shabgard and A. Faghri. Performance characteristics of cylindrical heat pipes with multiple heat sources. *Applied Thermal Engineering*, 31:3410–3419, 2011.

[8] S. Lips and F. Lefèvre. A general analytical model for the design of conventional heat pipes. *International Journal of Heat and Mass Transfer*, 72:288–298, 2014.

[9] N. Pooyoo, S. Kumar, J. Charoensuk, and A. Suksangpanomrung. Numerical simulation of cylindrical heat pipe considering non-darcian transport for liquid flow inside wick and mass flow rate at liquid-vapor interface. *International Journal of Heat and Mass Transfer*, 70:965–978, 2014.

[10] T. Brahim and A. Jemni. Effect of the heat pipe adiabatic region. *Journal of Heat Transfer*, 136:042901–1–10, 2014.

[11] T. Naemsai, N. Kammuang-lue, P. Terdtoon, and P. Sakulchangsatjatai. Numerical model of heat transfer characteristics for sintered-grooved wick heat pipes under non-uniform heat loads. *Applied Thermal Engineering*, 148:886–896, 2019.

[12] K. Grissa, A.M. Benselama, Z. Lataoui, C. Romestant, Y. Bertin, and A. Jemni. Performance of a cylindrical wicked heat pipe used in solar collectors: Numerical approach with lattice boltzmann method. *Energy Conversion and Management*, 150:623–636, 2017.

[13] N. Atabaki and B.R. Baliga. Effective thermal conductivity of water-saturated sintered powder-metal plates. *Heat and Mass Transfer*, 44:85–99, 2007.

[14] S.W. Chi. *Heat Pipe Theory and Practice*. Washington, D.C. : Hemisphere, 1976.

[15] D. Maillet, S. André, JC. Batsale, A. Degiovanni, and C. Moyne. *Thermal Quadrupoles : solving the heat equation through integral transforms*. John Wiley & Sons, Ltd, 2000.